Thermally modulated cross-stream migration of a surfactant-laden deformable drop in a Poiseuille flow

Sayan Das and Suman Chakraborty*

Department of Mechanical Engineering, Indian Institute of Technology Kharagpur, West Bengal 721302, India

A theoretical model is developed to study the cross-stream migration of a deformable surfactant-laden droplet suspended in a nonisothermal Poiseuille flow. In addition to the thermocapillary migration of the droplet, presence of shape deformation due to the imposed flow redistributes the surfactants along the interface that has a significant effect on its dynamics, which has yet remained unexplored. Owing to the nonlinearity present in the system of governing equations, an asymptotic approach is adopted to capture the intricate and nontrivial coupling between the various influencing parameters. Assuming negligible fluid inertia and thermal convection, the droplet migration velocity is obtained through small-deformation analysis in the limits of convective and diffusive surfactant transport. For the former limiting case, the droplet migrates towards the flow centerline when the temperature of the suspending medium increases in the direction of the imposed flow; however, the direction of its cross-stream migration reverses for a system with a high viscosity ratio of droplet to carrier phase. Under the same limiting scenario and for systems with low viscosity ratio, when the temperature linearly decreases in the direction of the imposed flow, the cross-stream migration velocity reduces with the increase in the applied temperature gradient till a critical point is reached at which there occurs no cross-stream migration. Beyond the critical point, there is a gradual increase in the magnitude of the cross-stream velocity with further rise in the imposed temperature gradient. The droplet, below the critical temperature gradient, migrates towards the flow centerline; however, above it the droplet moves away from the centerline. For the other limiting case where surfactant transport is dominated by surface convection, the magnitude of the cross-stream velocity is found to be significantly larger and at the same time independent of the droplet-carrier phase viscosity ratio.

I. INTRODUCTION

Manipulation of droplet motion in microchannels has attracted significant attention in the past few decades, due to its wide spread applications in different devices of practical importance [1–3]. A significant number of such applications are directed towards medical diagnostics and material-processing industries, including specific examples in drug delivery, cell encapsulation, reagent mixing, and analytic detection [1,4–7]. Some other relevant biological applications include the transverse migration and positioning of red blood cells and erythrocytes in the flow of blood through arteries [8,9]. A proper methodology for modulating the position of the dispersed phase (cells, droplets, or particles) has a wide scope in the domain of flow fractionation [10,11] and cytometry [12]. This control over the steady-state position of the droplet can be fine-tuned with

---

*suman@mech.iitkgp.ernet.in

the aid of an externally imposed temperature gradient, which can also be used for separation and sorting of droplets [13–15].

Several theoretical as well as experimental studies have been executed to analyze the dynamics of droplets that are transported with the helps of syringe pumps [16–18]. Haber and Hetsroni [19] theoretically demonstrated the migration characteristics of a surfactant-free Newtonian droplet suspended in an isothermal arbitrary Stokes flow. Later, the effect of different nonlinear effects such as shape deformation, inertia, and viscoelasticity were investigated [18,20,21]. It was shown that a deformable droplet, when placed eccentrically with respect to the centerline of a pressure driven, exhibits a migration in the cross-stream direction [20,22–26]. Chan and Leal [20] showed the effect of λ (which is the ratio of viscosity of the droplet phase to the carrier phase) on the cross-stream migration of the droplet. The cross-stream migration of the droplet is affected due to the presence of different external effects such as viscoelasticity [20,27,28] and fluid inertia [18,29,30], which introduces nonlinearity into the system. It has been shown experimentally that fluid inertia-induced lift force may drive a droplet away from the centerline of a microchannel [17]. Some recently published works have shown that cross-stream migration of a droplet occurs due to the presence of surfactants [31,32], even though there is no deformation, inertia, or viscoelasticity involved.

Surfactants are surface active agents which may be present as contaminants or may be externally added to stabilize an emulsion. Presence of an imposed flow results in a nonuniform distribution of surfactants along the droplet surface which significantly affects its dynamics by altering the surface tension [32,33]. The droplet deformation also results in surfactant redistribution that affects the surface tension gradient along the interface. There is experimental evidence which proves that there exists a relationship between the shape deformation and surfactant distribution along the droplet surface [34–36]. Stan *et al.* [17] showed numerically as well as experimentally that shape deformation of a surfactant-free droplet induces a lift force that significantly affects the cross-stream migration of the droplet. However, a significant number of studies have also analyzed the migration characteristics of a nondeformable surfactant-laden droplet [32]. Vlahovska *et al.* [37] used a small-deformation perturbation approach to show the effect of the Marangoni stress, generated due to nonuniform surfactant distribution, on the dynamics of a droplet suspended in a linear flow, for the limiting case where surfactant transport is dominated by surface convection.

A significant amount of research is directed towards proper modulation of the droplet or a particle in a flow field due to presence of different external effects such as magnetic [2], acoustic [2], electric [38–40], or temperature [41]. The first theoretical study to obtain the axial droplet migration velocity in a linearly varying temperature flow field was performed by Young *et al.* [42]. Later a number of researchers have studied thermocapillary motion of droplets in the presence of several nonlinear effects such as fluid inertia [43], droplet deformation [44], thermal convection [45–47], and bounding walls [48–52]. Sekhar *et al.* [53], in a recent work, studied the thermocapillary migration of droplet in the presence of an imposed Stokes flow where they showed that the effects due to imposed flow and thermocapillary action on fluid flow can be linearly combined in the absence of any shape deformation.

A number of studies have also shown the combined effect of thermocapillary and surfactant-induced Marangoni stress on droplet migration [54,55]. Recently Das *et al.* [56] showed the effect of temperature variation as well as surfactant distribution on the dynamics of a nondeformable droplet suspended in a Poiseuille flow. The present problem further extends this study by taking into account the effect of imposed flow-induced shape deformation on the cross-stream migration of the droplet. This problem is nonlinear and nontrivial and cannot be addressed as a mere superposition of the concerned influencing parameters, due to the unknown droplet shape. In order to tackle such a situation, we use an asymptotic approach for two limiting cases, namely, surface convection-driven-surfactant transport and surface diffusion-driven-surfactant transport. The prime objective of this study is to capture the mechanism and manner in which the imposed temperature gradient and shape deformation-induced surfactant redistribution alter the croos-stream migration characteristics of the droplet, which have hitherto not been addressed.
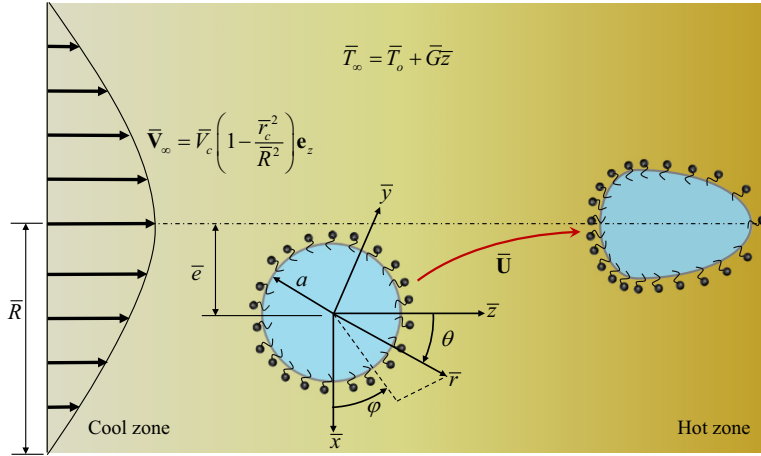
FIG. 1. Schematic of a surfactant-laden droplet of radius a suspended in a Poiseuille flow field. A linearly increasing temperature field ($\bar{T}_\infty$) in the direction of the imposed flow ($\bar{z}$ direction) is shown. The droplet is placed at an off-center position, $\bar{e}$ being the eccentricity. $\bar{R}$ is the distance from centerline of flow to the point of zero velocity. Both spherical ($\bar{r}$, θ, φ) as well as Cartesian coordinate system ($\bar{x}$, $\bar{y}$, $\bar{z}$) are shown. The $\bar{x}$ axis is directed away from the centerline of the droplet.

II. PROBLEM FORMULATION

A. System description

The present system consists of a neutrally buoyant Newtonian droplet of radius a suspended in another Newtonian fluid with an imposed Poiseuille flow. A schematic of the system is given in Fig. 1. The thermal conductivity and bulk viscosity of the droplet phase are denoted by k_i and η_i respectively. The respective properties for the suspending phase are k_e and η_e. It is assumed that a constant temperature gradient, $\bar{G}$, is applied to the suspending phase. Bulk insoluble surfactants are assumed to be present on the interface of the droplet. The surfactants gets transported only along the surface of the droplet by means of convection as well as diffusion. The only property which is not constant is the surface tension ($\bar{\sigma}$). The surface tension is directly dependent on the interfacial temperature $\bar{T}_s$ and the local surfactant concentration ($\bar{\Gamma}$). The equilibrium surface tension for a surfactant-free droplet is denoted by $\bar{\sigma}_c$ at a reference temperature of $\bar{T}_0$. In the absence of any imposed flow or temperature gradient, the surfactant is uniformly distributed along the droplet surface. The equilibrium surfactant concentration under such a situation is represented by $\bar{\Gamma}_{eq}$. The corresponding equilibrium surface tension is denoted by $\bar{\sigma}_{eq}$ that eventually changes to $\bar{\sigma}$ due to the disturbance generated by the imposed flow and a constant temperature gradient. The variation of temperature at the droplet interface generates a Marangoni stress which in conjunction with imposed flow-induced shape deformation results in further transport of the surfactants along the droplet surface. Thus the combined presence of an imposed Poiseuille flow and a linearly varying temperature field generates Marangoni stresses, which alters the migration velocity of the droplet ($\bar{U}$). The primary objective of the present study is to analyze the effect of the thermal Marangoni stresses on the cross-stream migration characteristics of the droplet. As can be seen from Fig. 1, we use a spherical coordinate system ($\bar{r}$, θ, φ) which is attached to the centroid of the droplet.

B. Important assumptions

Some of the important assumptions required to simplify the governing equations and boundary conditions for flow and temperature field are as follows:

(i) The transport of thermal energy by means of advection is neglected. That is, the thermal Péclet number for the present study is taken to be small, $Pe_T = \bar{V}_c a / \alpha_e \ll 1$, where α_e is the thermal diffusivity of the continuous phase and $\bar{V}_c$ is the centerline velocity of the imposed flow.

(ii) The effect of fluid inertia is assumed to be negligible, that is, the Reynolds number based on droplet radius is taken to be small $Re = \rho \bar{V}_c a / \mu_e \ll 1$, where ρ is the density of either of the phases.

(iii) Only small deformation of the droplet is taken into account. Thus the capillary number, $Ca^* = \mu_e \bar{V}_c / \bar{\sigma}_{eq}$, which is the ratio of the viscous force to the surface tension force acting on the droplet, is assumed to be small ($Ca^* \ll 1$).

(iv) The surfactants only get transported along the droplet surface and are insoluble in either of the phases [55].

(v) The surfactants are present as an ideal film at the interface and do not affect the heat transfer process [55].

(vi) The interfacial tension is linearly dependent on the surfactant concentration and the interfacial temperature distribution along the surface of the droplet through the equation of state [54–56].

(vii) Any effect of bounding walls is neglected, that is, the droplet is assumed to be suspended in an unbounded medium.

Typical values of the above nondimensional numbers, obtained from the experimental work of Chen *et al.* [57], show the above assumptions to be valid.

C. Governing equations and boundary conditions

The dimensionless form of the governing equations and relevant boundary conditions are now stated. The nondimensional scheme used for deriving these equations is

$$
\left.
\begin{aligned}
r &= \bar{r}/a, \ \mathbf{u} = \bar{\mathbf{u}}/\bar{V}_c, \ \Gamma = \bar{\Gamma}/\bar{\Gamma}_{eq}, \ \sigma = \bar{\sigma}/\bar{\sigma}_c, \\
p &= \bar{p}/(\mu_e \bar{V}_c/a), \ \boldsymbol{\tau} = \bar{\boldsymbol{\tau}}/(\mu_e \bar{V}_c/a), \ T = (\bar{T} - \bar{T}_o)/|\bar{G}|a,
\end{aligned}
\right\}
\tag{1}
$$

where all the quantities with an overbar represent dimensional quantities, and those without any overbar are dimensionless quantities. While deriving the governing equations and boundary conditions we encounter various nondimensional entities such as (i) the viscosity ratio, $\lambda = \mu_i/\mu_e$, which is the ratio of the viscosity of the droplet phase to that of the suspending phase; (ii) the thermal conductivity ratio, $\delta = k_i/k_e$, which is the ratio of the thermal conductivity of the droplet phase to that of the carrier phase; (iii) the elasticity number, $\beta = \bar{\Gamma}_{eq} R_g T_o / \bar{\sigma}_c = -d(\bar{\sigma}/\bar{\sigma}_c)/d\bar{\Gamma}$, which indicates the sensitivity of surface tension to the local surfactant concentration on the surface of the droplet; (iv) the thermal Marangoni number, $Ma_T = \gamma_T |\bar{G}|a/\mu_e \bar{V}_c$, which is the ratio of the thermocapillary-induced Marangoni stress to the viscous stress; (v) the surface Péclet number, $Pe_s = \bar{V}_c a / D_s$, which signifies the relative importance of surfactant transport due to advection to that due to surface diffusion, where D_s is the surface diffusivity of the surfactants; and (vi) the modified capillary number, $Ca = Ca^*/(1 - \beta)$, which is the ratio of the viscous force to the surface tension force acting on the droplet. From the definition of β, the equilibrium surface tension for a surfactant-laden droplet in the absence of any imposed flow or temperature gradient can be expressed as $\bar{\sigma}_{eq} = \bar{\sigma}_c(1 - \beta)$. Thus it is inevitable that the value of β lies within 1 and 0.

Based on the assumption of negligible convection of thermal energy, the dimensionless governing equations for the temperature field can be written as

$$
\left.
\begin{aligned}
\nabla^2 T_i &= 0, \\
\nabla^2 T_e &= 0,
\end{aligned}
\right\}
\tag{2}
$$

subjected to the following boundary conditions at the interface and at the far field:

$$\left.\begin{array}{l} \text{as } r \to \infty, \; T_e = \zeta r \cos\theta, \\ T_i \text{ is bounded at } r = 0, \\ \text{at } r = r_s, \quad T_i = T_e, \\ \text{at } r = r_s, \quad \delta(\boldsymbol{\nabla} T_i) \cdot \hat{\mathbf{n}} = (\boldsymbol{\nabla} T_e) \cdot \hat{\mathbf{n}}. \end{array}\right\} \tag{3}$$

The two boundary conditions at the interface indicate the continuity of temperature and heat transfer. Here T_i and T_e are the temperature field inside and outside the droplet. The quantity ζ indicates whether the droplet migrates in the direction of the imposed flow field or against it. If $\zeta = 1$, the temperature increases in the direction of the imposed flow, whereas $\zeta = -1$ signifies that the temperature decreases in the direction opposite to the direction of the imposed flow. The governing differential equations for the flow field can be expressed in a nondimensional form as follows [54,56]:

$$\left.\begin{array}{l} -\boldsymbol{\nabla} p_i + \lambda \nabla^2 \mathbf{u}_i = \mathbf{0}, \quad \boldsymbol{\nabla} \cdot \mathbf{u}_i = 0, \\ -\boldsymbol{\nabla} p_e + \nabla^2 \mathbf{u}_e = \mathbf{0}, \quad \boldsymbol{\nabla} \cdot \mathbf{u}_e = 0, \end{array}\right\} \tag{4}$$

where (u_i, u_e) and (p_i, p_e) are the velocity and pressure fields inside and outside the droplet. The relevant boundary conditions at the far field and at the interface of the droplet are the following:

$$\left.\begin{array}{l} \text{at } r \to \infty, \quad (\mathbf{u}_e, p_e) = (\mathbf{V}_\infty - \mathbf{U}, p_\infty), \\ \mathbf{u}_i \text{ is bounded at } r = 0, \\ \text{at } r = r_s, \; \mathbf{u}_i \cdot \hat{\mathbf{n}} = \mathbf{u}_e \cdot \hat{\mathbf{n}} = 0, \\ \text{at } r = r_s, \; \mathbf{u}_i = \mathbf{u}_e, \\ \text{at } r = r_s, \; (\boldsymbol{\tau}_e \cdot \hat{\mathbf{n}} - \boldsymbol{\tau}_i \cdot \hat{\mathbf{n}}) = \zeta \mathrm{Ma}_T \boldsymbol{\nabla}_s T + \frac{\beta}{(1-\beta)\mathrm{Ca}} \boldsymbol{\nabla}_s \Gamma + \frac{\sigma}{\mathrm{Ca}} (\boldsymbol{\nabla} \cdot \hat{\mathbf{n}}) \hat{\mathbf{n}}, \end{array}\right\} \tag{5}$$

where $r_s = 1 + \mathrm{Ca}\, g^{(\mathrm{Ca})}(\theta, \varphi) + \mathrm{Ca}^2 g^{(\mathrm{Ca}^2)}(\theta, \varphi)$. $g^{(\mathrm{Ca})}$ and $g^{(\mathrm{Ca}^2)}$ are $O(\mathrm{Ca})$ and $O(\mathrm{Ca}^2)$ correction to the shape of the droplet. Also $\mathbf{V}_\infty$ is the imposed circular Poiseuille flow field, $\mathbf{n}$ is the unit normal drawn on the droplet surface, and $\boldsymbol{\nabla}_s = (\mathbf{I} - \mathbf{nn})\boldsymbol{\nabla}$, is the surface gradient operator. The stress balance condition in Eq. (5) is obtained with the help of the following nondimensional equation of state:

$$\sigma = 1 - \zeta \mathrm{Ma}_T \mathrm{Ca} T_s - \beta \Gamma. \tag{6}$$

The dimensionless surfactant transport equation can be written as [58]

$$\mathrm{Pe}_s \boldsymbol{\nabla}_s \cdot (\mathbf{u}_s \Gamma) = \nabla_s^2 \Gamma. \tag{7}$$

The surfactants on the droplet surface must also fulfill the mass conservation constraint, which is given by

$$\int_{\varphi=0}^{2\pi} \int_{\theta=0}^{\pi} \Gamma(\theta, \varphi) \sin\theta \, d\theta \, d\varphi = 4\pi. \tag{8}$$

The temperature field, as observed from Eq. (2), is uncoupled from the flow field under the assumption of low thermal Péclet number. So temperature in either of the phases can be solved independently without solving for the flow field. However, this is not the situation when we try to obtain the solution for surfactant concentration as well as flow field. The flow field is coupled with both the temperature field as well as the surfactant distribution on the droplet surface, due to the presence of Marangoni stress. The surfactant concentration, on the other hand, is coupled to the flow field through the surfactant transport equation [Eq. (7)]. Thus a direct analytical solution is not possible. We thus use an asymptotic method which is performed for two limiting cases: (i) Low surface Péclet number, $\mathrm{Pe}_s \ll 1$, which signifies that the dominant mode of surfactant transport

is surface diffusion and (ii) high surface Péclet number, $\mathrm{Pe}_s \to \infty$, which indicates that surface advection is the main mode of surfactant transport along the droplet surface. Depending on the type surfactants used, the surface diffusivity may vary between $D_s = 10^{-11}$ and $10^{-8}\,\mathrm{m}^2/\mathrm{s}$ [59]. Based on a droplet of a radius 50 μm, the range of variation of Pe_s is given by $\mathrm{Pe}_s = 0.1 - 100$, which justifies the choice of the two limiting cases.

III. ASYMPTOTIC SOLUTION

A. Solution for $\mathrm{Pe}_s \ll 1$

As only a small deformation of the droplet is assumed, the order of magnitude of the surface Péclet number is taken to be the same as that of the capillary number, that is, $\mathrm{Pe}_s \sim \mathrm{Ca}$. This can be mathematically expressed as

$$\mathrm{Pe}_s = \kappa\mathrm{Ca}, \tag{9}$$

where $\kappa = a\bar{\sigma}_{\mathrm{eq}}(1-\beta)/\mu_e D_s$ is called the property parameter because it depends mainly on the material properties and has a finite magnitude. We thus in our asymptotic analysis choose Ca as the perturbation parameter. As we will be using the regular perturbation method to solve for the temperature and flow field, we can expand any generic variable (ψ) in a power series in terms of Ca in the following manner:

$$\psi = \psi^{(0)} + \psi^{(\mathrm{Ca})}\mathrm{Ca} + O(\mathrm{Ca}^2), \tag{10}$$

where $\psi^{(0)}$ is the leading order term corresponding to no deformation of the droplet and $\psi^{(Ca)}$ is $O(\mathrm{Ca})$ correction to the quantity, ψ, due to deformation of the droplet. Other terms indicate even higher order corrections due to droplet deformation. The surfactant concentration on the other hand is represented in the following manner:

$$\Gamma = 1 + \Gamma^{(0)}\mathrm{Ca} + \Gamma^{(\mathrm{Ca})}\mathrm{Ca}^2 + O(\mathrm{Ca}^3), \tag{11}$$

where $\Gamma^{(0)}$ and $\Gamma^{(\mathrm{Ca})}$ are $O(\mathrm{Ca})$ and $O(\mathrm{Ca}^2)$ correction to the surfactant concentration due to droplet deformation. The leading order contribution to the surfactant concentration ($\Gamma = 1$) signifies the scenario when the surfactants are uniformly distributed without any droplet deformation (Ca = 0).

First, with the help of Eq. (10), we derive the leading order and $O(\mathrm{Ca})$ boundary conditions for the temperature field. As the leading order governing equations and boundary conditions for temperature are not coupled with the flow field equations, the temperature field can be solved independently, whose expression is the same as was obtained by Das *et al.* [56]. Second, we obtain the leading order flow field boundary conditions, which along with the surfactant transport equation of the same order are solved for the velocity and the pressure field as well as the surfactant concentration. The leading order droplet migration velocity, which is obtained by the application of force-free condition, is

$$U_z^{(0)} = \begin{bmatrix} \frac{(3R^2-2)\kappa\beta+3(3\lambda R^2-2\lambda+2R^2)(1-\beta)}{3R^2\,\{\kappa\beta+(3\lambda+2)(1-\beta)\}} - \frac{e^2}{R^2} \\ +2\zeta\mathrm{Ma}_T\,\frac{(1-\beta)}{(\delta+2)\{\kappa\beta+(3\lambda+2)(1-\beta)\}} \end{bmatrix}, \quad U_x^{(0)} = U_y^{(0)} = 0, \tag{12}$$

where $U_z^{(0)}$ is the axial velocity of the droplet, whereas $U_x^{(0)}$, $U_y^{(0)}$ are the cross-stream migration velocity components. It can be inferred from the expression that there is no cross-stream migration of the droplet in the absence of droplet deformation. The leading order surfactant concentration, which satisfies the surfactant transport equation, is given by

$$\Gamma^{(0)} = \Gamma_{1,0}^{(0)}P_{1,0} + \Gamma_{3,0}^{(0)}P_{3,0} + \Gamma_{2,1}^{(0)}\cos\varphi\,P_{2,1},$$

$$\text{where} \quad \Gamma_{1,0}^{(0)} = \frac{1-\beta}{\{(3\lambda+2-\kappa)\beta - 3\lambda - 2\}}\left(\frac{3\kappa\mathrm{Ma}_T}{\delta+2} + \frac{2}{R^2}\right),$$

$$\Gamma_{3,0}^{(0)} = -\frac{7\kappa}{6R^2}\left\{\frac{1-\beta}{(7\lambda+7-\kappa)\beta-7\lambda-7}\right\}, \quad \Gamma_{2,1}^{(0)} = \frac{5e\kappa}{3R^2}\left\{\frac{1-\beta}{(5\lambda+5-\kappa)\beta-5\lambda-5}\right\}. \quad (13)$$

Third, with the leading order solution at hand, the $O(\text{Ca})$ correction to droplet shape, $g^{(\text{Ca})}$, is obtained with the help of the normal stress boundary condition as

$$g^{(\text{Ca})} = L_{3,0}^{(\text{Ca})} P_{3,0} + L_{2,1} \cos\varphi P_{2,1},$$

where

$$L_{2,1}^{(\text{Ca})} = -\frac{5e}{12R^2}\left\{\frac{4\kappa\beta+(16+19\lambda)(1-\beta)}{\kappa\beta+5(1+\lambda)(1-\beta)}\right\}, \quad L_{3,0}^{(\text{Ca})} = \frac{7}{60R^2}\left\{\frac{5\kappa\beta+3(11\lambda+10)(1-\beta)}{\kappa\beta+7(1+\lambda)(1-\beta)}\right\}. \quad (14)$$

It can be inferred from the above expression that the $O(\text{Ca})$ shape deformation of the droplet is independent of the interfacial temperature gradient or the thermal Marangoni stress (Ma_T). However the surfactant distribution is altered as a result of the thermally induced Marangoni stress, which can be seen from Eq. (13). This variation in interfacial surfactant concentration, which is coupled with the flow field through the surfactant transport equation [Eq. (7)], alters the fluid flow and hence the migration velocity of the droplet. We now proceed towards determining the $O(\text{Ca})$ temperature field ($T_i^{(\text{Ca})}$, $T_e^{(\text{Ca})}$), flow field ($\mathbf{u}_{i,e}^{(\text{Ca})}$, $p_{i,e}^{(\text{Ca})}$), and the surfactant concentration ($\Gamma^{(\text{Ca})}$) by repeating the above steps over the boundary conditions evaluated at the deformed interface.

The expression for the $O(\text{Ca})$ temperature field, thus obtained, is

$$\left.\begin{array}{l} T_i^{(\text{Ca})} = \sum_{n=0}^{4}\sum_{m=0}^{n}\left[a_{n,m}^{(\text{Ca})} r^n \cos(m\varphi) + \hat{a}_{n,m}^{(\text{Ca})} r^n \sin(m\varphi)\right] P_{n,m}(\cos\theta), \\[2mm] T_e^{(\text{Ca})} = \sum_{n=0}^{4}\sum_{m=0}^{n}\left[b_{-n-1,m}^{(\text{Ca})} r^{-n-1} \cos(m\varphi) + \hat{b}_{-n-1,m}^{(\text{Ca})} r^{-n-1} \sin(m\varphi)\right] P_{n,m}(\cos\theta), \end{array}\right\} \quad (15)$$

where the constant coefficients are given in Sec. III A of the Supplemental Material [60].

The expressions for the axial and the cross-stream component of velocities are

$$U_z^{(\text{Ca})} = 0, \quad U_y^{(\text{Ca})} = 0, \quad U_x^{(\text{Ca})} = \frac{e}{c_3(\beta,\kappa,\lambda,\delta)}[c_1(\beta,\kappa,\lambda,\delta) + \zeta\text{Ma}_T c_2(\beta,\kappa,\lambda,\delta)], \quad (16)$$

where the constants c_1, c_2, and c_3 in the above expression is given in Sec. III B of the Supplemental Material [60]. As can be seen from the above expression for cross-stream migration velocity, the thermal Marangoni stress explicitly has an effect on the cross-stream migration velocity of the droplet even though a constant temperature gradient is applied in the axial direction. This is quite nonintuitive.

Finally, the expression for $O(\text{Ca})$ surfactant concentration is given by

$$\Gamma^{(\text{Ca})} = \begin{bmatrix} \Gamma_{0,0}^{(\text{Ca})} + \Gamma_{1,1}^{(\text{Ca})} \cos\varphi P_{1,1} + \Gamma_{2,0}^{(\text{Ca})} P_{2,0} + \Gamma_{2,2}^{(\text{Ca})} \cos(2\varphi) P_{2,2} \\ +\Gamma_{3,1}^{(\text{Ca})} \cos\varphi P_{3,1} + \Gamma_{4,0}^{(\text{Ca})} P_{4,0} + \Gamma_{4,2}^{(\text{Ca})} \cos(2\varphi) P_{4,2} \end{bmatrix}, \quad (17)$$

where $\Gamma_{0,0}^{(\text{Ca})}$ is obtained from the relation for mass conservation of surfactants as given in Eq. (8). The detailed expressions of the constant coefficients in the above equation are extremely lengthy and hence not presented here.

B. Solution for $\text{Pe}_s \gg 1$

Unlike the limiting case of low Péclet number, we have $\text{Pe}_s^{-1} \sim \text{Ca}$ for the case of high surface Péclet number. The main difference from the previous case lies in the surfactant transport equation, which for the present limiting case becomes [55]

$$\nabla_s \cdot (\mathbf{u}_s \Gamma) = 0. \quad (18)$$

All the quantities in this case are expanded in a power series with respect to Ca, as was done in the previous case. A similar approach is followed for this limiting case too. Hence only the important results are highlighted without getting into the details of the methodology. The temperature field for the leading order of perturbation is the same as was obtained for the case of $\mathrm{Pe}_s \ll 1$. The leading order as well as $O(\mathrm{Ca})$ droplet migration velocity for $\mathrm{Pe}_s \gg 1$ is given by

$$U_z^{(0)} = \left(1 - \frac{2}{3R^2}\right) - \frac{e^2}{R^2}, \quad U_x^{(0)} = U_y^{(0)} = 0,$$

$$\text{and } U_z^{(\mathrm{Ca})} = U_y^{(\mathrm{Ca})} = 0, \quad U_x^{(\mathrm{Ca})} = -e\left[\frac{4 - 3\beta}{6R^4\beta} + \zeta\mathrm{Ma}_T\left\{\frac{1 - \beta}{R^2(\delta + 2)\beta}\right\}\right]. \tag{19}$$

As can be seen from the above expression of $O(\mathrm{Ca})$ cross-stream migration velocity, the thermal Marangoni stress has a direct effect on the cross-stream migration of the droplet, although the temperature gradient is applied in the axial direction. The leading order and $O(\mathrm{Ca})$ surfactant concentration as obtained from the surfactant transport equation are

$$\Gamma^{(0)} = \Gamma_{1,0}^{(0)}P_{1,0} + \Gamma_{3,0}^{(0)}P_{3,0} + \Gamma_{2,1}^{(0)}\cos\varphi P_{2,1}$$

where $\Gamma_{1,0}^{(0)} = -\left(1 - \frac{1}{\beta}\right)\left(\frac{3\mathrm{Ma}_T}{\delta + 2} + \frac{2}{R^2}\right), \quad \Gamma_{3,0}^{(0)} = -\frac{7}{6R^2}\left(1 - \frac{1}{\beta}\right), \quad \Gamma_{2,1}^{(0)} = -\frac{5e}{3R^2}\left(1 - \frac{1}{\beta}\right),$

and $\quad \Gamma^{(\mathrm{Ca})} = \begin{bmatrix} \Gamma_{0,0}^{(\mathrm{Ca})} + \Gamma_{1,1}^{(\mathrm{Ca})}\cos\varphi P_{1,1} + \Gamma_{2,0}^{(\mathrm{Ca})}P_{2,0} + \Gamma_{2,2}^{(\mathrm{Ca})}\cos(2\varphi)P_{2,2} \\ +\Gamma_{3,1}^{(\mathrm{Ca})}\cos\varphi P_{3,1} + \Gamma_{4,0}^{(\mathrm{Ca})}P_{4,0} + \Gamma_{4,2}^{(\mathrm{Ca})}\cos(2\varphi)P_{4,2} \end{bmatrix}, \tag{20}$

where all the constant coefficients in the above equation are provided in Sec. III D of the Supplemental Material [60]. The expression for $\Gamma_{0,0}^{(\mathrm{Ca})}$ can easily be obtained with the help of the mass conservation constraint as given in Eq. (8). The $O(\mathrm{Ca})$ correction to the droplet shape, $g^{(\mathrm{Ca})}$, as obtained from the normal stress boundary condition, is

$$g^{(\mathrm{Ca})} = L_{2,1}^{(\mathrm{Ca})}\cos\varphi P_{2,1} + L_{3,0}^{(\mathrm{Ca})}P_{3,0}, \text{ where } L_{2,1} = -\frac{5}{3}\frac{e}{R^2}, \ L_{3,0} = \frac{7}{12R^2}. \tag{21}$$

On solving the boundary conditions for temperature field at the deformed droplet surface ($r_s = 1 + g^{(\mathrm{Ca})}\mathrm{Ca}$), we obtain the $O(\mathrm{Ca})$ temperature distribution inside and outside the droplet as

$$\left.\begin{array}{l} T_i^{(\mathrm{Ca})} = \sum\limits_{n=0}^{4}\sum\limits_{m=0}^{n}\left[p_{n,m}^{(\mathrm{Ca})}r^n\cos(m\varphi) + \hat{p}_{n,m}^{(\mathrm{Ca})}r^n\sin(m\varphi)\right]P_{n,m}(\cos\theta), \\ T_e^{(\mathrm{Ca})} = \sum\limits_{n=0}^{4}\sum\limits_{m=0}^{n}\left[q_{-n-1,m}^{(\mathrm{Ca})}r^{-n-1}\cos(m\varphi) + \hat{q}_{-n-1,m}^{(\mathrm{Ca})}r^{-n-1}\sin(m\varphi)\right]P_{n,m}(\cos\theta), \end{array}\right\} \tag{22}$$

where the constant coefficients are provided in Sec. III C of the Supplemental Material [60].

IV. DISCUSSION OF RESULTS

The prime result of our analysis is the droplet cross-stream migration velocity for the two limiting cases: (i) low surface Péclet number limit ($\mathrm{Pe}_s \ll 1$) and (ii) high surface Péclet number limit. We first begin our discussion with the low surface Péclet number limit ($\mathrm{Pe}_s \to \infty$).

A. Low surface Péclet limit

In this limiting condition the surfactant transport is primarily dominated by surface diffusion rather than interfacial advection of surfactants. The present study focuses on the variation of the steady-state cross-stream migration velocity of the droplet (U_x). The expression for the cross-stream
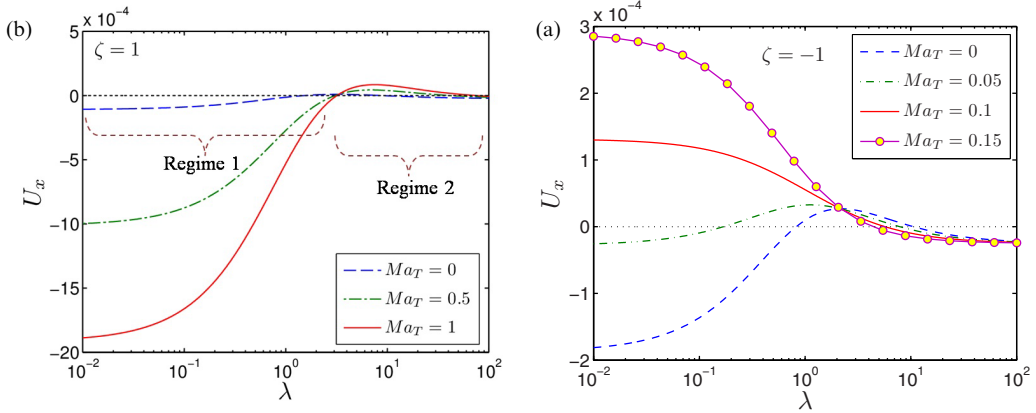
FIG. 2. Variation of cross-stream migration velocity of the droplet (U_x) with λ for different values of Ma_T. (a) Here the temperature increases in the direction of imposed Poiseuille flow ($\zeta = 1$), whereas in (b) the temperature decreases in the direction of the imposed flow ($\zeta = -1$). The other parameters are $\delta = 1$, $\beta = 0.5$, $\kappa = 3$, $R = 5$, $e = 1$, and $\mathrm{Ca} = 0.1$.

migration velocity of the droplet in this limit is

$$\mathbf{U}_x = \mathrm{Ca}\,\frac{e}{c_3(\beta, \kappa, \lambda, \delta)}[c_1(\beta, \kappa, \lambda, \delta) + \zeta \mathrm{Ma}_T c_2(\beta, \kappa, \lambda, \delta)]\mathbf{e}_x. \tag{23}$$

It is seen from Eq. (16) that there is no effect of shape deformation on the axial migration velocity of the droplet. Hence no further investigation on the same is done. Towards providing a detailed analysis on the cross-stream migration of the droplet, we first show the variation of U_x with the viscosity ratio, λ, for different values of thermal Marangoni number (Ma_T) in Fig. 2. We consider two different cases of applied thermal gradient, namely, a linearly increasing temperature field in the direction of the imposed flow ($\zeta = 1$) and a linearly decreasing temperature field in the same direction ($\zeta = -1$).

1. Increase in temperature in the direction of the imposed Poiseuille flow ($\zeta = 1$)

It can be seen from Fig. 2(a) that for the case of a droplet suspended in an isothermal flow ($\mathrm{Ma}_T = 0$), the cross-stream migration velocity decreases with increase in the viscosity ratio, λ. For a sufficiently high viscous droplet, there is negligible cross-stream migration of the droplet. On the other hand, if an axial temperature gradient is externally imposed, the cross-stream migration velocity increases. For low values of λ, there is a significant effect of the applied temperature gradient on the cross-stream migration velocity of the droplet, but it gradually fades away as λ is increased. This is because the jump in the tangential stress across the interface is significantly higher for the case of a low viscous droplet. For a nonisothermal system, the variation of the droplet cross-stream migration velocity with λ follows the same trend as seen for $\mathrm{Ma}_T = 0$. It should also be noted that there is an inflexion point present. That is, the droplet continues to migrate towards the centerline of flow as long as $\lambda < 2.5$, depending on the other nondimensional parameters which have been given in the caption of Fig. 2. This region has been named "regime 1" of the flow. Above $\lambda = 2.5$, the direction of cross-stream droplet migration changes, that is, it starts migrating away from the flow centerline although the cross-stream velocity still increases with increase in the axially applied temperature gradient (or Ma_T). This region of flow where the direction of transverse migration of the droplet reverses is named "regime 2" of the flow. It should be noted that even though the temperature gradient is applied in the axial direction, the cross-stream migration of the droplet is affected. This is highly nonintuitive. On comparison with the study done by Das *et al.* [56], where the droplet was considered to be nondeformable, it can be seen that in the present study a deformable droplet may
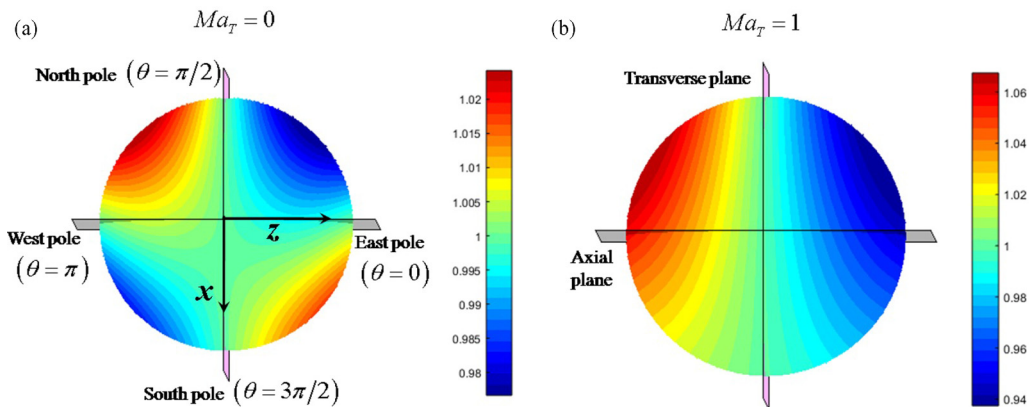
FIG. 3. Contour plot of the surfactant distribution ($\tilde{\Gamma}$) on the droplet surface for two cases: (a) the droplet is suspended in an isothermal flow field ($\mathrm{Ma}_T = 0$) and (b) the droplet is suspended in a nonisothermal flow field with the temperature increasing in the direction of the imposed flow ($\mathrm{Ma}_T = 1$). The other parameter values are $\delta = 1$, $\beta = 0.5$, $\lambda = 0.1$, $\kappa = 3$, $R = 5$, $e = 1$, and $\mathrm{Ca} = 0.1$.

change its direction of cross-stream migration depending on the viscosity ratio of the system (λ), even for the special case of $\zeta = 1$.

In order to provide a physical insight to nature of variation in cross-stream migration velocity, we first show the surfactant distribution along the droplet surface in the form of a contour plot in Figs. 3(a) and 3(b). Figure 3(a) shows the surfactant distribution for an isothermal flow field, whereas Fig. 3(b) highlights the effect of a positive temperature gradient on the surfactant concentration and hence on the droplet dynamics. It can be seen from both Figs. 3(a) and 3(b) that the surfactant distribution is plotted on the surface of an undeformed spherical droplet. This is done by projecting the surfactant distribution on a deformed droplet to a undeformed spherical surface of the droplet in the following form: $\tilde{\Gamma} = \Gamma(r_s^2/\mathbf{n} \cdot \mathbf{r})$ [31]. The sole reason for this transformation is to avoid the complexity of expressing the surface divergence vector on a deformed droplet. As our focus is primarily on the cross-stream migration of the droplet, we look into the surfactant distribution on either sides of the axial plane of the droplet. It can be seen from both Figs. 3(a) and 3(b) that there is a clear asymmetry in surfactant distribution across the axial plane. This is due to the eccentrically placed droplet in a Poiseuille flow as a result of which there exists unequal surface velocities along its northern and southern hemispheres. For instance, consider the system shown in Fig. 1. As the droplet is placed below the centerline of flow, the upper hemisphere has a higher surface velocity as compared to the lower hemisphere, which is responsible for this asymmetry in surfactant distribution.

For the present limiting case of $\zeta = 1$, there is fluid flow from the east pole to the west pole along the droplet surface. A higher surface velocity in the northern hemisphere results in a larger surfactant concentration on the northwest part of the droplet as compared to the northeast portion [see Fig. 3(a)]. The lower hemisphere, which has a lower surface velocity, has a higher concentration of surfactants on the southeast portion of the droplet. This asymmetry in surfactant distribution across the axial plane generates a gradient in the surface tension along any transverse plane of the droplet, which in turn results in the creation of a Marangoni stress, responsible for the retardation of the cross-stream migration of the droplet [32,33]. The asymmetric distribution of surfactants and its transport along the droplet surface also significantly affects the normal stress balance and hence the associated droplet deformation [33,37]. Deformation of the droplet redistributes the surfactants along the droplet surface, which alters the Marangoni stress and hence affects the droplet dynamics. When a temperature gradient is applied in the direction of imposed flow [see Fig. 3(b)], a thermal Marangoni stress is developed that opposes the Marangoni stress generated due to the nonuniform
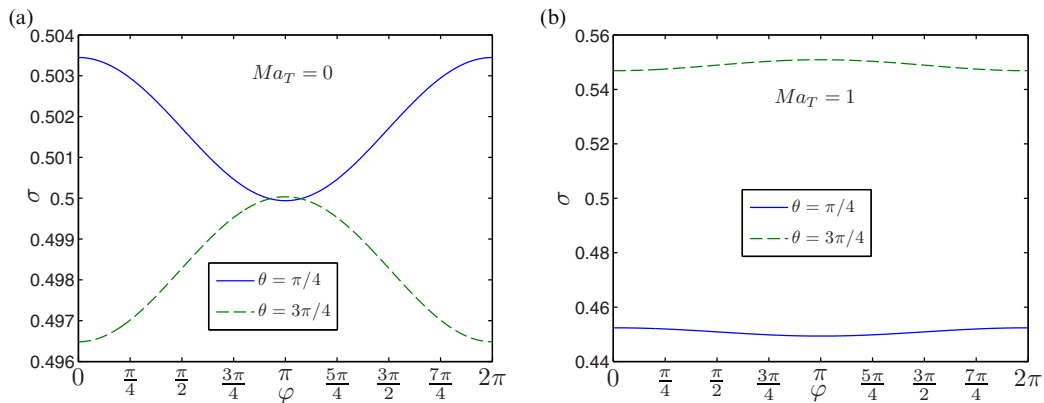
FIG. 4. Variation of surface tension along two different planes which are parallel to and are located on either sides of the axial plane, for two cases: (a) the droplet is suspended in an isothermal flow field and (b) the droplet is suspended in a nonisothermal flow field with the temperature increasing in the direction of the imposed flow ($Ma_T = 1$). The parameter values are $\delta = 1, \beta = 0.5, \lambda = 0.1, \kappa = 3, R = 5, e = 1$, and $Ca = 0.1$.

distribution of surfactants and forces the droplet to migrate towards the hotter region of the flow field. This increases the net convective transport of surfactants due to enhanced interfacial fluid flow as compared the case of an isothermal flow field, which in turn results in an enhanced asymmetry in surfactant distribution. As can be seen from comparison of Figs. 3(b) and 3(a), there is a significant increase in the gradient in surfactant concentration ($|\Gamma_{max} - \Gamma_{min}|$) when a constant temperature gradient is applied in the direction of bulk flow, which results in a net increase in the surface tension gradient ($|\sigma_{max} - \sigma_{min}|$) over the droplet surface [refer to Figs. 4(a) and 4(b)]. Both these figures show the variation of surface tension along two axial planes at two different transverse positions ($\theta = \pi/4, 3\pi/4$) for an isothermal and a nonisothermal system, respectively. From Fig. 4(a) it is evitable that the surface tension is higher along the northern hemisphere, whereas its magnitude is comparatively lower along the lower hemisphere. This generates a surfactant Marangoni stress that acts in a direction away from the flow centerline and hence opposes the imposed flow-driven cross-stream migration of the droplet towards the center. However, in Fig. 4(b), presence of a constant temperature gradient in the direction of the imposed flow results in a higher surface tension along the lower hemisphere, which indicates that the net Marangoni stress acts in a direction towards the centerline of flow, thus aiding droplet migration.

Hence the cross-stream migration velocity increases. Further increase in the temperature gradient increases the net Marangoni stress, which in turn enhances the cross-stream velocity. This, in fact, can be observed from Fig. 2(a) in regime 1. For regime 2, a high enough value of λ, alters the surfactant distribution along the droplet surface resulting a net change in the overall Marangoni stress, which now drives the droplet away from the flow centerline [Fig. 2(b)]. In this regime too, increase in the temperature gradient is manifested by a rise in the magnitude of the cross-stream migration velocity of the droplet.

2. Decrease in temperature in the direction of the imposed Poiseuille flow ($\zeta = -1$)

We next discuss on the special case of a linearly decreasing temperature field in the direction of imposed bulk flow ($\zeta = -1$). Figure 2(b) shows the variation of cross-stream migration velocity with viscosity ratio, λ. In this scenario too, the droplet initially, for low values of λ, migrates towards the centerline of flow, provided that the applied temperature gradient is sufficiently low (low Ma_T). Unlike the previous case of $\zeta = 1$, the cross-stream migration velocity of the droplet in this case reduces as the temperature gradient is increased. This decrease in the cross-stream migration
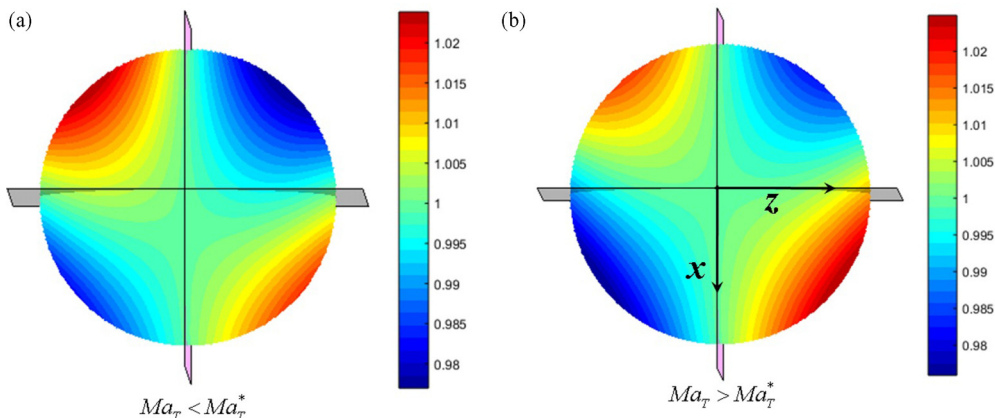
FIG. 5. Contour plot of the surfactant distribution ($\tilde{\Gamma}$) on the droplet surface for the case when the temperature linearly decreases along the direction of the imposed flow ($\zeta = -1$). The plot is been shown for two cases: (a) $Ma_T < Ma_T{}^*$ and (b) $Ma_T > Ma_T{}^*$. The parameter values are $\delta = 1$, $\beta = 0.5$, $\lambda = 0.1$, $\kappa = 3$, $R = 5$, $e = 1$, and $Ca = 0.1$.

velocity of the droplet continues till a point is reached where there is no more lateral migration. This is the critical point, and the corresponding thermal Marangoni number is known as the critical thermal Marangoni number, $Ma_T{}^*$. Increase of Ma_T beyond this critical value results in a reversal in the direction of the cross-stream migration of the droplet, which now migrates away from flow centerline. The expression for $Ma_T{}^*$ corresponding to zero cross-stream migration can be obtained from Eq. (23):

$$Ma_T^* = \frac{c_1}{c_2}. \tag{24}$$

Thus any increase in the imposed temperature gradient, in this region, results in an increase in the magnitude of the cross-stream velocity of the droplet. This behavior can be seen for the case of low-viscous droplets ($\lambda < 2$). On the contrary for $\lambda > 2$, that is, for high-viscous droplets, the behavior of the cross-stream migration of the droplet was noted to be just the opposite. Initially for the droplets with $\lambda \approx 2$, the cross-stream migration velocity reduces with increase in both λ as well as Ma_T, and the droplet migrates away from the centerline of flow. On further increase in λ, the droplet starts behaving as a particle, and there remains no effect of Marangoni stress on the droplet dynamics. At such high values of λ, the variation of cross-stream migration velocity, due to change in Ma_T, becomes negligible and results in droplet migration towards the flow centerline with a larger cross-stream migration velocity, irrespective of the value of Ma_T.

For a better understanding, we show the distribution of surfactants on the droplet surface [$\tilde{\Gamma}(\theta,\varphi)$] for $Ma_T < Ma_T{}^*$ and $Ma_T > Ma_T{}^*$ in a contour plot in Figs. 5(a) and 5(b), respectively. For the present scenario ($\zeta = -1$), the thermally induced Marangoni stress drives the surfactants from the west pole to the east pole of the droplet, whereas the bulk Poiseuille flow forces the surfactants to migrate from the east to the west pole. Thus the interfacial fluid flow, induced by the imposed flow and the applied temperature gradient oppose each other. Further surfactant redistribution also takes place due to droplet deformation. Hence, depending on whether the Marangoni stress due to imposed flow or the applied temperature gradient dominates, the interfacial fluid flow may be from the west pole to the east pole or in the opposite direction. This net surface velocity along with the surfactant redistribution due to droplet deformation decides the direction as well as magnitude of the cross-stream migration velocity. For the case when the thermal Marangoni stress is less than its critical counterpart, the Marangoni convection due to the imposed Poiseuille flow dominates. Thus fluid flow takes place from the east to the west pole. Taking into account the nonuniformity in
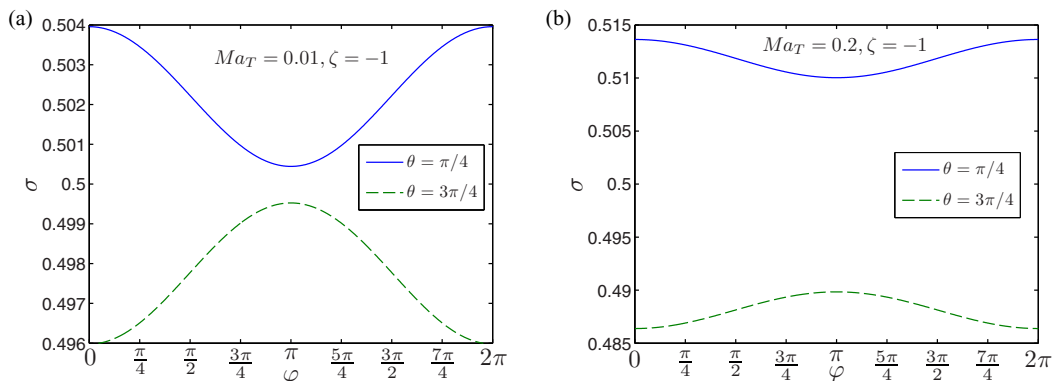
FIG. 6. Variation of surface tension along two planes ($\theta = \pi/4, 3\pi/4$) parallel to and located on either sides of the axial plane for the case when the temperature decreases in the direction of the imposed flow. In panel (a) $\mathrm{Ma}_T < \mathrm{Ma}_T{}^*$, and in panel (b) $\mathrm{Ma}_T < \mathrm{Ma}_T{}^*$. The parameter values are $\delta = 1$, $\beta = 0.5$, $\lambda = 0.1$, $\kappa = 3$, $R = 5$, $e = 1$, and $\mathrm{Ca} = 0.1$.

the surface velocity along both the hemispheres of the droplet due to its eccentric positioning, the highest surfactant concentration is expected in the northwest region of the droplet surface, and the minimum surfactant concentration in the northeast region. This is exactly what is seen in Fig. 5(a). It can be seen that Fig. 5(a) is quite similar to that shown in Fig. 3(b). Hence the droplet, for the case of $\mathrm{Ma}_T < \mathrm{Ma}_T{}^*$, migrates towards the center line of flow. For the other case where $\mathrm{Ma}_T > \mathrm{Ma}_T{}^*$, the thermal Marangoni stress dominates and the direction of the surface velocity reverses. This results in a maximum surfactant concentration in the southeast region of the droplet, as shown in Fig. 5(b). On comparison with Fig. 5(a), the surfactant distribution is found to be just the opposite for this scenario. Hence the direction of the cross-stream migration alters, and it starts migrating away from the flow centerline, as was shown in Fig. 2(b).

Figures 6(a) and 6(b) show the variation of $\sigma(\theta, \varphi)$ along two planes on either side of the axial plane at transverse positions, $\theta = \pi/4, 3\pi/4$. First, on comparison with Fig. 4(a), it can be seen that the net surface tension gradient, $|\sigma_{\max} - \sigma_{\min}|$, is higher for the case $\mathrm{Ma}_T < \mathrm{Ma}_T{}^*$. Also it is the upper droplet surface which has the higher surface tension as compared to the lower surface.

Thus the net Marangoni stress developed acts away from the flow centerline. Since for this scenario the imposed Poiseuille flow dominates the interfacial fluid flow, the enhanced Marangoni stress due to increase in the surface tension gradient in comparison to the case of an isothermal flow ($\mathrm{Ma}_T = 0$) opposes the cross-stream migration of the droplet towards the flow centerline even more. As a consequence, the cross-stream migration velocity reduces with increase in Ma_T as long as $\mathrm{Ma}_T < \mathrm{Ma}_T{}^*$ although the droplet migrates towards the axial plane. This can be seen in Fig. 2(b). For the special case when $\mathrm{Ma}_T > \mathrm{Ma}_T{}^*$, the thermally induced Marangoni stress dominates the interfacial fluid flow, and hence the net Marangoni stress, this time, succeeds in driving the droplet away from the flow center line. With rise in Ma_T, the surface tension gradient increases, which indicates a net increase in the Marangoni stress. Thus further increase in Ma_T enhances the cross-stream migration velocity of the droplet, which now migrates away from axial plane.

B. High surface Péclet limit

Under this limit, the surfactant transport is along the interface and is dominated by the surface convection. The cross-stream migration velocity of the droplet for the limiting case of high Pe_s is
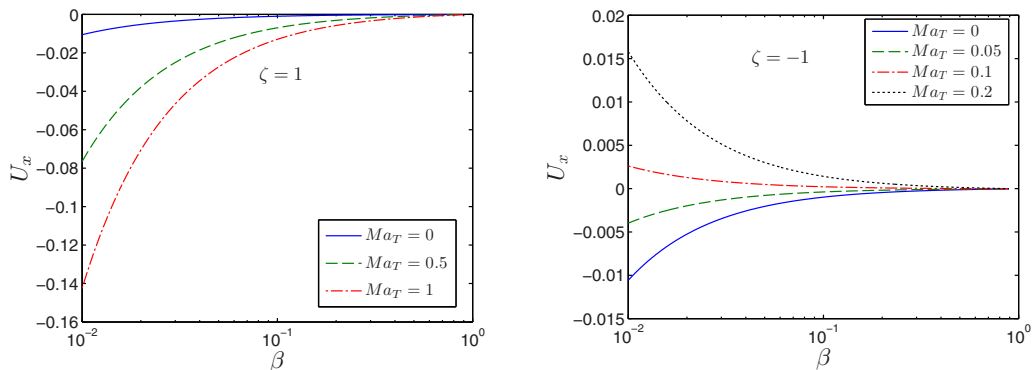
FIG. 7. Variation of cross-stream migration velocity (U_x) with β for different values of Ma$_T$. (a) Here the applied temperature gradient increases in the direction of imposed Poiseuille flow ($\zeta = 1$). The values of Ma$_T$ are 0, 0.5, and 1. (b) Here the applied temperature gradient decreases in a direction of the imposed flow ($\zeta = 1$). The values of Ma$_T$ are 0, 0.05, 0.1, and 0.2. The other parameters are $\delta = 1$, $\beta = 0.5$, $R = 5$, $e = 1$, and Ca = 0.1.

given by

$$\mathbf{U}_x = -e\mathrm{Ca}\left[\frac{1}{6R^4}\left(\frac{4-3\beta}{\beta}\right) + \frac{\zeta \mathrm{Ma}_T}{R^2(\delta+2)}\left\{\frac{1-\beta}{\beta}\right\}\right]\mathbf{e}_x. \tag{25}$$

It can be inferred from the above expression that shape deformation play an important role in the cross-stream migration of the droplet. There is no presence of cross-stream migration velocity for the leading order solution. Since β lies between 0 and 1, the above expression clearly indicates that the droplet always migrates towards the flow centerline when the temperature increases in the direction of the imposed flow ($\zeta = 1$), which is unlike the case for the low Péclet number limit. However, for an applied temperature gradient in the opposite direction ($\zeta = -1$), the droplet may either migrate towards or away from the flow centerline. In the absence of λ in the above expression of cross-stream migration velocity, we show the variation of the same with β for different values of Ma$_T$ in Fig. 7.

1. Increase in temperature in the direction of imposed flow ($\zeta = 1$)

Figure 7 shows the variation of U_x as a function of β for two separate cases: $\zeta = 1$ [Fig. 7(a)] and $\zeta = -1$ [Fig. 7(b)]. Each of the plots is shown for different values of Ma$_T$. Under this scenario ($\zeta = 1$) it can be observed from Fig. 7(a) that increase in β reduces the cross-stream migration velocity of the droplet irrespective of the applied temperature gradient. This is due to the fact that rise in β actually increases the surfactant-induced Marangoni stress along the droplet interface that acts against the direction of the imposed flow and hence reduces the net cross-stream migration velocity of the droplet [33]. In the presence of an imposed axial temperature gradient, the cross-stream migration velocity follows the same trend as in the low Péclet limit. However, the magnitude of the cross-stream migration velocity is much larger as compared to the former limiting case due to surface convection-dominated surfactant transport. It can also be seen from Fig. 7(a) that the impact of Ma$_T$ on the cross-stream migration velocity of the droplet reduces with increase in β. A higher value of β results in an increased asymmetry in the surface tension across the axial plane and hence a larger surfactant-induced Marangoni stress, which nullifies the positive effect of the thermally induced Marangoni stress.

Towards obtaining a physical insight, we next show a contour plot on the distribution of the surfactants along the surface of the droplet in Fig. 8. It is to be noted from comparison between Fig. 8(a) and Fig. 3(a) that asymmetry in the surfactant distribution across the axial plane is higher
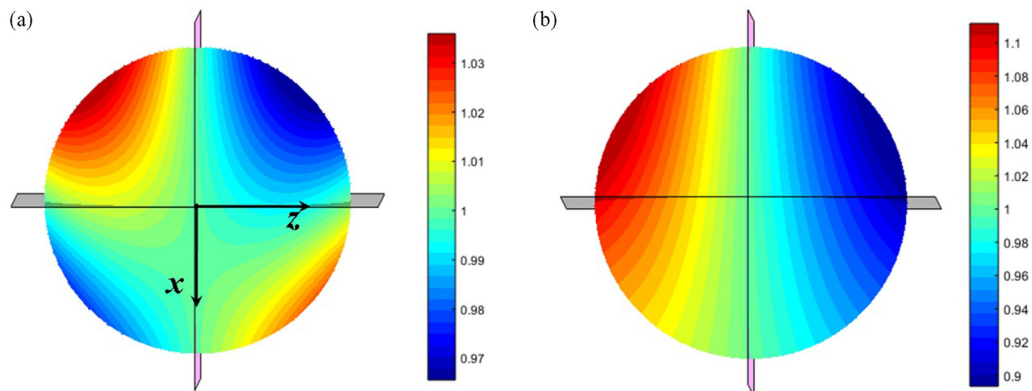
FIG. 8. Contour plot of the surfactant distribution ($\tilde{\Gamma}$) on the droplet surface for two cases: (a) isothermal flow field ($\mathrm{Ma}_T = 0$) and (b) nonisothermal flow field with the temperature increasing in the direction of the imposed flow ($\mathrm{Ma}_T = 1$). The contour plot is shown for the limitng case of $\mathrm{Pe}_s \to \infty$. The parameter values are $\delta = 1$, $\beta = 0.5$, $\lambda = 0.1$, $R = 5$, $e = 1$, and $\mathrm{Ca} = 0.1$.

for the limiting case of high Péclet number even for an isothermal flow field due to enhanced convection-driven surfactant transport. Similar is the case for a nonisothermal flow field [Fig. 8(b)], where also the asymmetry in surfactant distribution along the droplet surface ($|\Gamma_{\max} - \Gamma_{\min}|$) is larger for the present limiting case. As the temperature increases in the direction of the bulk flow, there is an interfacial fluid flow from the east pole to the west pole of the droplet, which together with the surface velocity due to the imposed flow results in the highest surfactant concentration along the northwest region of the droplet and lowest in the northeast region. Since the distribution pattern of the surfactants is similar to the limiting case of low Péclet number, the droplet in this scenario migrates towards the flow centerline. Increase in ($|\Gamma_{\max} - \Gamma_{\min}|$) and hence in ($|\sigma_{\max} - \sigma_{\min}|$) for a droplet suspended in a nonisothermal flow field results in an enhanced net Marangoni stress that drives the droplet towards the centerline of flow with a higher cross-stream migration velocity. This explains the fact that an axially applied temperature gradient can significantly increase the cross-stream migration velocity of a droplet.

2. Decrease in temperature in the direction of imposed fluid flow ($\zeta = -1$)

We refer to Fig. 7(b), where the variation of the cross-stream migration velocity is shown for this scenario. Increase in β always results in a reduction of the cross-stream migration velocity, irrespective of the magnitude of the applied temperature gradient (or Ma_T). Similarly to the previous limiting case for $\mathrm{Pe}_s \ll 1$, we again define a critical Marangoni number, $\mathrm{Ma}_T{}^*$, which denotes the critical point above which the droplet migrates away from the flow centerline and below which it moves towards the centerline of flow. At this critical point there is no cross-stream migration of the droplet. Keeping this in mind the expression of $\mathrm{Ma}_T{}^*$ can be derived and expressed as

$$\mathrm{Ma}_T^* = \frac{(\delta + 2)}{6R^2}\left(3 + \frac{1}{1-\beta}\right). \tag{26}$$

As long as $\mathrm{Ma}_T < \mathrm{Ma}_T{}^*$, any increase in the temperature gradient and hence Ma_T results in a reduction in the magnitude of the cross-stream migration velocity. However, in the regime of $\mathrm{Ma}_T < \mathrm{Ma}_T$, the cross-stream migration velocity gradually increases with increase in Ma_T and at the same time migrates away from the flow centerline. The effect of Ma_T on the cross-stream migration of the droplet reduces with increase in β for this case too.

A better understanding can be obtained from Figs. 9(a) and 9(b) which show the surfactant concentration along the droplet surface for the two special cases of $\mathrm{Ma}_T < \mathrm{Ma}_T{}^*$ and $\mathrm{Ma}_T > \mathrm{Ma}_T{}^*$
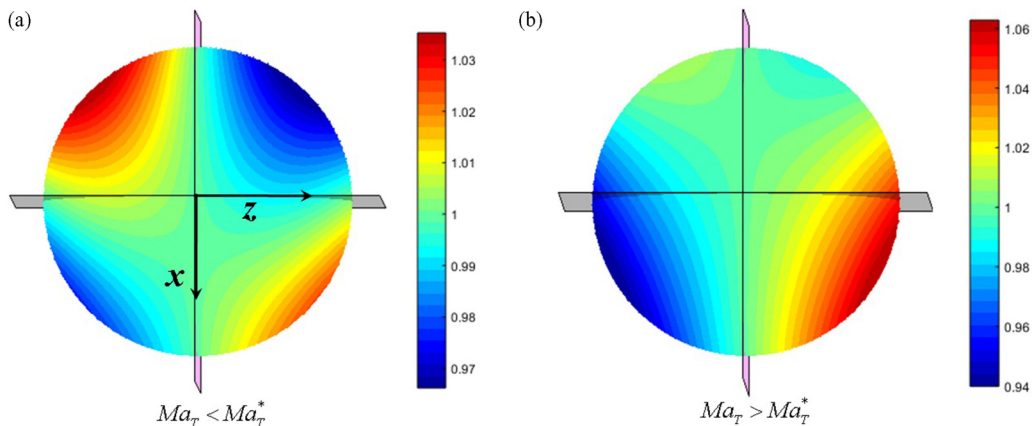
FIG. 9. Contour plot of the surfactant distribution ($\tilde{\Gamma}$) on the droplet surface for two scenarios: (a) $Ma_T = 0.01$ and (b) $Ma_T = 0.5$. The figures are shown for the case of linearly decreasing temperature in the direction of imposed flow and for the limiting case of high surface Péclet number ($Pe_s \rightarrow \infty$). The parameter values are $\delta = 1$, $\beta = 0.5$, $\lambda = 0.1$, $R = 5$, $e = 1$, and $Ca = 0.1$.

respectively. When $Ma_T < Ma_T^*$ [Fig. 9(a)], the imposed flow dominates over the thermocapillary effect, and hence there is a net flow from the east pole to the west. Since the droplet is eccentrically located, the highest surfactant concentration is on the northwestern region of the droplet while the minimum concentration is present in the northeastern domain. Similar surfactant distribution, as shown in Fig. 8(a), suggests that the droplet should migrate towards the flow centerline. On the other hand, when the thermocapillary effect dominates due to a high-temperature gradient $Ma_T > Ma_T^*$, the fluid flow along the droplet surface reverses and the highest surfactant concentration is on the southeastern region [see Fig. 5(b)]. This suggests that the droplet migrates away from the centerline of flow.

C. Comparison of our results with previously published work

Here we compare the magnitude of cross-stream migration velocity obtained under both the limiting conditions, with the results of some of the previously published studies. These studies include the analysis performed by Chan *et al.* [20], where they obtained the cross-stream migration velocity of a deformable droplet in an unbounded Poiseuille flow. They considered neither the effect of any external temperature gradient nor the presence of any surfactants. Later, Das *et al.* [56] considered the effect of both surfactants and an imposed temperature gradient on the cross-stream migration of a spherical (or nondeformable) droplet. Recently, Das *et al.* [33] studied the effect of deformation and surfactant distribution on the motion of a droplet in an isothermal Poiseuille flow. Here we take into consideration the combined effect of both an external temperature gradient and shape deformation on the lateral migration of a surfactant-laden droplet in a Poiseuille flow. The presence of both surfactants and shape deformation introduces nonlinearity into the mathematical model, which makes it impossible to obtain the cross-stream migration velocity by a linear superposition of the results from the above problems. The different values of the cross-stream migration velocity as obtained from the present study as well from the work done by Chan *et al.* [20] and Das *et al.* [33,56] are tabulated below.

As can be seen from Table I that under the presence of the a constant axial temperature gradient as well as consideration of droplet deformation results in a significant rise in the magnitude of the cross-stream migration velocity of the droplet. The values of the different parameters used for this evaluation are $Ca = 0.05$, $Pe_s = 0.1$, $\delta = 1$, $R = 5$, $e = 1$, $\kappa = 1$, and $\beta = 0.5$. For the high Péclet number limit we have used $Pe_s = 10$.

TABLE I. Comparison of the magnitude of cross-stream migration velocity with previous works.

Different studies	Cross-stream velocity (U_x)	
	$Pe_s \ll 1$	$Pe_s \gg 1$
Cross-stream migration of a surfactant-free deformable droplet in an isothermal Poiseuille flow [20]	1.205×10^{-4}	
Cross-stream migration of a surfactant-laden nondeformable droplet in a nonisothermal Poiseuille flow [56]	4.828×10^{-4}	10.057×10^{-4}
Cross-stream migration of a surfactant-laden deformable droplet in an isothermal Poiseuille flow [33]	0.68×10^{-4}	0.667×10^{-4}
Present study	6.317×10^{-4}	10.19×10^{-4}

V. REMARKS

In the present study, an asymptotic analysis is performed for the two limiting cases of low and high Pe_s. Mathematically speaking, the governing equations and the corresponding boundary conditions are impossible to linearize for the case of medium Pe_s. This is because the velocity field and the surfactant concentration always remains coupled to each other in the surfactant transport equation, which adds to the nonlinearity present due to the unknown shape of the droplet. However, a qualitative prediction can be made regarding the migration velocity of the droplet for a medium value of Pe_s based on different literatures [55,61–63]. The magnitude of the droplet velocity will always lie in between the velocities corresponding to the two limiting case of low ($Pe_s \ll 1$) and high Péclet number ($Pe_s \rightarrow \infty$). However, the trend in variation of droplet velocity with different parameters (say, λ) will remain similar. Since the magnitude of the droplet migration velocity will increase for $Pe_s = O(1)$ as compared to the limiting case of $Pe_s \ll 1$, it is expected that the critical thermal Marangoni stress, required to nullify the droplet migration, will also increase, provided all the other parameters remain constant.

VI. CONCLUSIONS

The present study deals with the cross-stream migration of a surfactant-laden droplet suspended in a Poiseuille flow with a linearly increasing temperature gradient. The droplet is taken to be deformable; however, only small deviations from the spherical shape are assumed. The system under consideration is taken to neutrally buoyant, and any presence of inertia in fluid flow is neglected. We use a asymptotic approach to solve the nonlinear system of governing equations and relevant boundary conditions under two different limiting cases, namely, surface-diffusion-dominated and surface-convection-dominated transport of surfactants. Since the system of governing equations and boundary conditions are all highly nonlinear and coupled due to the consideration of droplet deformation and associated surfactant redistribution, a linear superposition of the results of a thermocapillary-driven and an imposed flow actuated migration of a surfactant-laden droplet may give erroneous predictions. We obtain the droplet migration velocity as well as the surfactant concentration along the droplet surface till $O(Ca)$. The thermocapillary effect on droplet cross-stream migration is analyzed for two specific cases: one in which the temperature increases linearly in the direction of the imposed flow ($\zeta = 1$) and the other where the direction of the applied temperature gradient is reversed ($\zeta = -1$). After a thorough analysis of the droplet migration characteristics, some of the important findings established are the following:

Firstly, for the limiting case of low surface Péclet number, the droplet, in general, always migrates towards the centerline of flow. It is seen that increase in the axial temperature gradient results in increase in the cross-stream migration velocity of the droplet, provided the temperature increases in

the direction of the imposed flow. For high-viscosity ratios, the direction the droplet cross-stream migration reverses depending on the value of Ma_T.

Secondly, when the temperature decreases in the direction of the imposed Poiseuille flow, the droplet may migrate towards or away from the flow centerline depending on the magnitude of the applied temperature gradient as well as the droplet viscosity. For a low-viscous droplet, the droplet migrates towards the flow centerline, and the magnitude of the cross-stream migration velocity reduces with increase in Ma_T till $Ma_T < Ma_T{}^*$. However, at the critical point $Ma_T = Ma_T{}^*$, there is no cross-stream migration. Beyond this critical value ($Ma_T{}^*$) any further increase in Ma_T results in an increase in the magnitude of the cross-stream migration velocity. The droplet now migrates away from the flow centerline. A highly viscous droplet, on the other hand, always migrates towards the centerline of flow.

Thirdly, for the limiting case of high surface Péclet number limit, the magnitude of the cross-stream migration velocity is always higher as compared to the limiting case of low surface Péclet number. The nature of variation of the steady-state cross-stream velocity with Ma_T is the same as that for the low Péclet number limit, but it is independent of the droplet viscosity.

[1] C. N. Baroud, F. Gallaire, and R. Dangla, Dynamics of microfluidic droplets, Lab Chip **10**, 2032 (2010).

[2] R. Seemann, M. Brinkmann, T. Pfohl, and S. Herminghaus, Droplet based microfluidics, Rep. Prog. Phys. **75**, 16601 (2012).

[3] H. A. Stone, A. D. Stroock, and A. Ajdari, Engineering flows in small devices: Microfluidics toward a lab-on-a-chip, Annu. Rev. Fluid Mech. **36**, 381 (2004).

[4] S.-Y. Teh, R. Lin, L.-H. Hung, and A. P. Lee, Droplet microfluidics, Lab Chip **8**, 198 (2008).

[5] A. Huebner, S. Sharma, M. Srisa-Art, F. Hollfelder, J. B. Edel, and A. J. Demello, Microdroplets: A sea of applications?, Lab Chip **8**, 1244 (2008).

[6] D. Di Carlo, D. Irimia, R. G. Tompkins, and M. Toner, Continuous inertial focusing, ordering, and separation of particles in microchannels, Proc. Natl. Acad. Sci. USA **104**, 18892 (2007).

[7] Y. Zhu and Q. Fang, Analytical detection techniques for droplet microfluidics—A review, Anal. Chim. Acta **787**, 24 (2013).

[8] T. M. Geislinger and T. Franke, Hydrodynamic lift of vesicles and red blood cells in flow—From Fåhræus & Lindqvist to microfluidic cell sorting, Adv. Colloid Interface Sci. **208**, 161 (2014).

[9] A. Pries, T. Secomb, and P. Gaehtgens, Biophysical aspects of blood flow in the microvasculature, Cardiovasc. Res. **32**, 654 (1996).

[10] J. Giddings, Field-flow fractionation: Analysis of macromolecular, colloidal, and particulate materials, Science **260**, 1456 (1993).

[11] J. Yang, Y. Huang, X.-B. Wang, F. F. Becker, and P. R. C. Gascoyne, Cell separation on microfabricated electrodes using dielectrophoretic/gravitational field-flow fractionation, Anal. Chem. **71**, 911 (1999).

[12] W. A. Bonner, H. R. Hulett, R. G. Sweet, and L. A. Herzenberg, Fluorescence activated cell sorting, Rev. Sci. Instrum. **43**, 404 (1972).

[13] C. N. Baroud, J.-P. Delville, F. Gallaire, and R. Wunenburger, Thermocapillary valve for droplet production and sorting, Phys. Rev. E **75**, 046302 (2007).

[14] M. Robert, D. S. Vincent, R. Wunenburger, J. Delville, M. Robert, D. S. Vincent, R. Wunenburger, and J. Delville, Laser switching and sorting for high speed digital microfluidics, Appl. Phys. Lett. **92**, 154105 (2008).

[15] V. Miralles, A. Huerre, F. Malloggi, and M. Jullien, A review of heating and temperature control in microfluidic systems: Techniques and applications, Diagnostics **3**, 33 (2013).

[16] L. G. Leal, Particle motions in a viscous fluid, Annu. Rev. Fluid Mech. **12**, 435 (1980).

[17] C. A. Stan, L. Guglielmini, A. K. Ellerbee, D. Caviezel, H. A. Stone, and G. M. Whitesides, Sheathless hydrodynamic positioning of buoyant drops and bubbles inside microchannels, Phys. Rev. E **84**, 036302 (2011).

[18] X. Chen, C. Xue, L. Zhang, G. Hu, X. Jiang, and J. Sun, Inertial migration of deformable droplets in a microchannel, Phys. Fluids **26**, 112003 (2014).

[19] G. Hetsroni and S. Haber, The flow in and around a droplet or bubble submerged in an unbound arbitrary velocity field, Rheol. Acta **9**, 488 (1970).

[20] P. C.-H. Chan and L. G. Leal, The motion of a deformable drop in a second-order fluid, J. Fluid Mech. **92**, 131 (1979).

[21] B. P. Ho and L. G. Leal, Inertial migration of rigid spheres in two-dimensional unidirectional flows, J. Fluid Mech. **65**, 365 (1974).

[22] S. Haber and G. Hetsroni, The dynamics of a deformable drop suspended in an unbounded Stokes flow, J. Fluid Mech. **49**, 257 (1971).

[23] P. R. Wohl and S. I. Rubinow, The transverse force on a drop in an unbounded parabolic flow, J. Fluid Mech. **62**, 185 (1974).

[24] S. Mortazavi and G. Tryggvason, A numerical study of the motion of drops in Poiseuille flow. Part 1. Lateral migration of one drop, J. Fluid Mech. **411**, 325 (2000).

[25] A. J. Griggs, A. Z. Zinchenko, and R. H. Davis, Low-Reynolds-number motion of a deformable drop between two parallel plane walls, Int. J. Multiph. Flow **33**, 182 (2007).

[26] S. Mandal, A. Bandopadhyay, and S. Chakraborty, Effect of interfacial slip on the cross-stream migration of a drop in an unbounded Poiseuille flow, Phys. Rev. E **92**, 023002 (2015).

[27] S. Mukherjee and K. Sarkar, Effects of matrix viscoelasticity on the lateral migration of a deformable drop in a wall-bounded shear, J. Fluid Mech. **727**, 318 (2013).

[28] S. Mukherjee and K. Sarkar, Lateral migration of a viscoelastic drop in a Newtonian fluid in a shear flow near a wall, Phys. Fluids **26**, 103102 (2014).

[29] A. Karnis, H. L. Goldsmith, and S. G. Mason, The flow of suspensions through tubes V. Inertial effects, Can. J. Chem. Eng. **44**, 181 (1966).

[30] S. C. Hur, N. K. Henderson-MacLennan, E. R. B. McCabe, and D. Di Carlo, Deformability-based cell classification and enrichment using inertial microfluidics, Lab Chip **11**, 912 (2011).

[31] P. M. Vlahovska, M. Loewenberg, and J. Blawzdziewicz, Deformation of a surfactant-covered drop in a linear flow, Phys. Fluids **17**, 103103 (2005).

[32] O. S. Pak, J. Feng, and H. A. Stone, Viscous Marangoni migration of a drop in a Poiseuille flow at low surface Péclet numbers, J. Fluid Mech. **753**, 535 (2014).

[33] S. Das, S. Mandal, and S. Chakraborty, Cross-stream migration of a surfactant-laden deformable droplet in a Poiseuille flow, Phys. Fluids **29**, 82004 (2017).

[34] P. Van Puyvelde, S. Velankar, and P. Moldenaers, Rheology and morphology of compatibilized polymer blends, Curr. Opin. Colloid Interface Sci. **6**, 457 (2001).

[35] Y. T. Hu and A. Lips, Estimating Surfactant Surface Coverage and Decomposing its Effect on Drop Deformation, Phys. Rev. Lett. **91**, 044501 (2003).

[36] H. K. Jeon and C. W. Macosko, Visualization of block copolymer distribution on a sheared drop, Polymer (Guildf). **44**, 5381 (2003).

[37] P. M. Vlahovska, J. Błlawzdziewicz, and M. Loewenberg, Small-deformation theory for a surfactant-covered drop in linear flows, J. Fluid Mech. **624**, 293 (2009).

[38] K. Ahn, C. Kerbage, T. P. Hunt, R. M. Westervelt, D. R. Link, and D. A. Weitz, Dielectrophoretic manipulation of drops for high-speed microfluidic sorting devices, Appl. Phys. Lett. **88**, 24104 (2006).

[39] D. R. Link, E. Grasland-Mongrain, A. Duri, F. Sarrazin, Z. Cheng, G. Cristobal, M. Marquez, and D. A. Weitz, Electric control of droplets in microfluidic devices, Angew. Chemie Intl. Ed. **45**, 2556 (2006).

[40] A. Bandopadhyay, S. Mandal, N. K. Kishore, and S. Chakraborty, Uniform electric-field-induced lateral migration of a sedimenting drop, J. Fluid Mech. **792**, 553 (2016).

[41] A. Karbalaei, R. Kumar, and H. J. Cho, Thermocapillarity in microfluidics—A review, Micromachines **7**, 13 (2016).

[42] N. O. Young, J. S. Goldstein, and M. J. Block, The motion of bubbles in a vertical temperature gradient, J. Fluid Mech. **6**, 350 (1959).

[43] H. Haj-Hariri, A. Nadim, and A. Borhan, Effect of inertia on the thermocapillary velocity of a drop, J. Colloid Interface Sci. **140**, 277 (1990).

[44] A. Nadim, H. Haj-Hariri, and A. Borhan, Thermocapillary migration of slightly deformed droplets, Part. Sci. Technol. **8**, 191 (1990).

[45] R. Balasubramaniam and R. S. Subramanian, Thermocapillary convection due to a stationary bubble, Phys. Fluids **16**, 3131 (2004).

[46] E. Yariv and M. Shusser, On the paradox of thermocapillary flow about a stationary bubble, Phys. Fluids **18**, 072101 (2006).

[47] L. Zhang, R. S. Subramanian, and R. Balasubramaniam, Motion of a drop in a vertical temperature gradient at small Marangoni number—The critical role of inertia, J. Fluid Mech. **448**, 197 (2001).

[48] M. Meyyappan and R. S. Subramanian, Thermocapillary migration of a gas bubble in an arbitrary direction with respect to a plane surface, J. Colloid Interface Sci. **115**, 206 (1987).

[49] K. D. Barton and R. Shankar Subramanian, Thermocapillary migration of a liquid drop normal to a plane surface, J. Colloid Interface Sci. **137**, 170 (1990).

[50] K. D. Barton and R. S. Subramanian, Migration of liquid drops in a vertical temperature gradient-interaction effects near a horizontal surface, J. Colloid Interface Sci. **141**, 146 (1991).

[51] S. H. Chen, Thermocapillary deposition of a fluid droplet normal to a planar surface, Langmuir **15**, 2674 (1999).

[52] S. H. Chen, Thermocapillary coagulations of a fluid sphere and a gas bubble, Langmuir **19**, 4582 (2003).

[53] D. Choudhuri and G. P. Raja Sekhar, Thermocapillary drift on a spherical drop in a viscous fluid, Phys. Fluids **25**, 043104 (2013).

[54] S. Das, S. Mandal, S. K. Som, and S. Chakraborty, Migration of a surfactant-laden droplet in non-isothermal Poiseuille flow, Phys. Fluids **29**, 12002 (2017).

[55] H. S. Kim and R. S. Subramanian, The thermocapillary migration of a droplet with insoluble surfactant: II. General case, J. Colloid Interface Sci. **130**, 112 (1989).

[56] S. Das, S. Mandal, and S. Chakraborty, Effect of temperature gradient on the cross-stream migration of a surfactant-laden droplet in Poiseuille flow, J. Fluid Mech. **835**, 170 (2018).

[57] Y. S. Chen, Y. L. Lu, Y. M. Yang, and J. R. Maa, Surfactant effects on the motion of a droplet in thermocapillary migration, Int. J. Multiph. Flow **23**, 325 (1997).

[58] S. Mandal, S. Das, and S. Chakraborty, Effect of Marangoni stress on the bulk rheology of a dilute emulsion of surfactant-laden deformable droplets in linear flows, Phys. Rev. Fluids **2**, 113604 (2017).

[59] K. J. Stebe, S. Y. Lin, and C. Maldarelli, Remobilizing surfactant retarded fluid particle interfaces. 1. Stress-free conditions at the interfaces of micellar solutions of surfactants with fast sorption kinetics, Phys. Fluids A **3**, 3 (1991).

[60] See Supplemental Material at http://link.aps.org/supplemental/10.1103/PhysRevFluids.3.103602 for the details regarding the governing equations, the boundary conditions, and the asymptotic approach adopted in this study to obtain the temperature and the flow field.

[61] C. Pozrikidis, A finite-element method for interfacial surfactant transport, with application to the flow-induced deformation of a viscous drop, J. Eng. Math. **49**, 163 (2004).

[62] C. Kallendorf, A. Fath, M. Oberlack, and Y. Wang, Exact solutions to the interfacial surfactant transport equation on a droplet in a Stokes flow regime, Phys. Fluids **27**, 082104 (2015).

[63] S. Mandal, A. Bandopadhyay, and S. Chakraborty, Dielectrophoresis of a surfactant-laden viscous drop, Phys. Fluids **28**, 62006 (2016).